

## Article

# Microstructures of HfO<sub>x</sub> Films Prepared via Atomic Layer Deposition Using La(NO<sub>3</sub>)<sub>3</sub>·6H<sub>2</sub>O Oxidants

Seon Yong Kim <sup>1</sup>, Yong Chan Jung <sup>1,2</sup>, Sejong Seong <sup>1</sup>, Taehoon Lee <sup>1</sup>, In-Sung Park <sup>3,\*</sup> and Jinho Ahn <sup>1,3,\*</sup>

<sup>1</sup> Division of Materials Science and Engineering, Hanyang University, Seoul 04763, Korea; tjsdyd93@hanyang.ac.kr (S.Y.K.); Yongchan.Jung@utdallas.edu (Y.C.J.); sejongseong@gmail.com (S.S.); lth911218@gmail.com (T.L.)

<sup>2</sup> Department of Materials Science and Engineering, The University of Texas at Dallas, Richardson, TX 75080, USA

<sup>3</sup> Institute of Nano Science and Technology, Hanyang University, Seoul 04763, Korea

\* Correspondence: parkis77@hanyang.ac.kr (I.-S.P.); jhahn@hanyang.ac.kr (J.A.)

**Abstract:** Hafnium oxide (HfO<sub>x</sub>) films have a wide range of applications in solid-state devices, including metal–oxide–semiconductor field-effect transistors (MOSFETs). The growth of HfO<sub>x</sub> films from the metal precursor tetrakis(ethylmethylamino) hafnium with La(NO<sub>3</sub>)<sub>3</sub>·6H<sub>2</sub>O solution (LNS) as an oxidant was investigated. The atomic layer deposition (ALD) conditions were optimized, and the chemical state, surface morphology, and microstructure of the prepared films were characterized. Furthermore, to better understand the effects of LNS on the deposition process, HfO<sub>x</sub> films deposited using a conventional oxidant (H<sub>2</sub>O) were also prepared. The ALD process using LNS was observed to be self-limiting, with an ALD temperature window of 200–350 °C and a growth rate of 1.6 Å per cycle, two times faster than that with H<sub>2</sub>O. HfO<sub>x</sub> films deposited using the LNS oxidant had smaller crystallites than those deposited using H<sub>2</sub>O, as well as more suboxides or defects because of the higher number of grain boundaries. In addition, there was a difference in the preferred orientations of the HfO<sub>x</sub> films deposited using LNS and H<sub>2</sub>O, and consequently, a difference in surface energy. Finally, a film growth model based on the surface energy difference was proposed to explain the observed growth rate and crystallite size trends.

**Keywords:** hafnium oxide film; atomic layer deposition; MOSFET



**Citation:** Kim, S.Y.; Jung, Y.C.; Seong, S.; Lee, T.; Park, I.-S.; Ahn, J. Microstructures of HfO<sub>x</sub> Films Prepared via Atomic Layer Deposition Using La(NO<sub>3</sub>)<sub>3</sub>·6H<sub>2</sub>O Oxidants. *Materials* **2021**, *14*, 7478. <https://doi.org/10.3390/ma14237478>

Academic Editor: Christian Müller

Received: 8 November 2021

Accepted: 4 December 2021

Published: 6 December 2021

**Publisher's Note:** MDPI stays neutral with regard to jurisdictional claims in published maps and institutional affiliations.



**Copyright:** © 2021 by the authors. Licensee MDPI, Basel, Switzerland. This article is an open access article distributed under the terms and conditions of the Creative Commons Attribution (CC BY) license (<https://creativecommons.org/licenses/by/4.0/>).

## 1. Introduction

Recently, hafnium oxide (HfO<sub>x</sub>) thin films have been studied as promising electronic materials for a wide range of solid-state device applications. The excellent insulating and dielectric properties of HfO<sub>x</sub> enable its application in semiconductor devices. Thin films based on HfO<sub>x</sub> have substituted SiO<sub>2</sub> as the material of choice for the gate dielectric layer in metal–oxide–semiconductor field-effect transistors (MOSFETs) because of their high dielectric constant, wide band gap, large band offset, and good thermodynamic stability on Si wafers [1]. More recently, HfO<sub>x</sub> has been widely studied as a candidate insulating layer in resistors with metal–insulator–metal structures, which are used in non-volatile resistive switching memory [2]. Furthermore, HfO<sub>x</sub> doped with La and Zr has attracted attention for use in CMOS-compatible ferroelectric devices [3,4]. The dopants distort the structure of HfO<sub>x</sub>, generating a ferroelectric polar orthorhombic structure.

With the continued reduction in size and increase in complexity of semiconductor devices, a need for the fabrication of ultrathin films with precisely controlled thickness on three-dimensional device structures is becoming apparent. To meet this requirement, atomic layer deposition (ALD) is one possible thin film fabrication method [5]. To fabricate metal oxide films, a typical ALD cycle consists of four steps: pulsing the metal precursor, purging the remnant with inert gas, pulsing the oxidant, and purging the remnant with inert gas. ALD via the above basic process has the advantage of offering precisely controlled

of ultrathin layers with good uniformity, as well as excellent conformal coating of surfaces with intricate structures [6].

However, because of the extremely slow growth rate in ALD, low productivity is a serious disadvantage. To enhance the throughput of the ALD method, many studies have been focused on developing batch-type ALD and spatial ALD [7,8]. In particular, both metal precursors and oxidants can modulate the characteristics of metal oxide films; that is, the choice of these materials influences the growth rate, ALD temperature window, crystalline structure, contamination, and dielectric and electrical properties. Various oxidants have been used to prepare ALD oxide films, such as  $\text{H}_2\text{O}$ ,  $\text{H}_2\text{O}_2$ ,  $\text{O}_3$ , and plasma-based radical oxygen [1,9]. In addition to the precursor and oxidant, the catalyst can strongly affect the deposition properties and material characteristics of films grown by ALD. To fabricate  $\text{ZrO}_2$  films, Oh et al. used  $\text{La}(\text{NO}_3)_3 \cdot 6\text{H}_2\text{O}$  solution instead of  $\text{H}_2\text{O}$  as an oxidant and compared the crystalline phase, grain size, and surface roughness of the resulting  $\text{ZrO}_2$  films [10]. Interestingly, use of the  $\text{La}(\text{NO}_3)_3 \cdot 6\text{H}_2\text{O}$  solution increased the  $\text{ZrO}_2$  film growth rate because of a catalytic effect of the La-based oxidant. In addition,  $\text{HfO}_2$  films deposited with  $\text{La}(\text{NO}_3)_3 \cdot 6\text{H}_2\text{O}$  solution instead of  $\text{H}_2\text{O}$  exhibited modified resistive switching characteristics [11]. However, in those studies, characterization of the specific ALD processes involved when a solution oxidant is used, in terms of self-saturation, ALD temperature window, and growth linearity, was lacking. In addition, the suggested mechanism did not adequately explain the origins of the microstructural differences observed. Accordingly, in this study, a  $\text{La}(\text{NO}_3)_3 \cdot 6\text{H}_2\text{O}$  solution was used as an oxidant for ALD, with the aim of optimizing the ALD process.

In this work, we focused on the use of  $\text{La}(\text{NO}_3)_3 \cdot 6\text{H}_2\text{O}$  as a catalytic oxidant in the ALD of  $\text{HfO}_x$  films. The properties of these films were compared with those of  $\text{HfO}_x$  films fabricated via ALD using  $\text{H}_2\text{O}$  as an oxidant; the film thickness was monitored as a function of precursor and oxidant pulse time, deposition temperature, and the number of ALD cycles. The chemical, surface morphological, and structural properties of the deposited  $\text{HfO}_x$  films were analyzed by X-ray photoelectron spectroscopy (XPS), atomic force microscopy (AFM), grazing-incidence X-ray diffraction (GI-XRD), and transmission electron microscopy (TEM). Furthermore, a deposition mechanism was proposed to explain the difference between the growth properties and microstructures of  $\text{HfO}_2$  films fabricated using the  $\text{La}(\text{NO}_3)_3 \cdot 6\text{H}_2\text{O}$  solution and  $\text{H}_2\text{O}$ .

## 2. Materials and Methods

### 2.1. $\text{HfO}_x$ Film Fabrication

$\text{HfO}_x$  thin films were deposited on Si(100) substrates by ALD using tetrakis (ethylmethylamino) hafnium (TEMAH) as the metal precursor and 40 wt%  $\text{La}(\text{NO}_3)_3 \cdot 6\text{H}_2\text{O}$  solution (LNS) as an oxidant. To better understand the effects of LNS,  $\text{HfO}_x$  thin films were also prepared using  $\text{H}_2\text{O}$  as the oxidant, and the deposition and material properties of these were compared with those of the thin films prepared using LNS. Prior to the deposition of the  $\text{HfO}_x$  thin films, p-type Si(100) substrates were cleaned in a dilute HF solution to remove the native oxide film. The metal precursor, TEMAH, was volatilized at 60 °C and delivered into a vacuum chamber filled with a pure  $\text{N}_2$  carrier gas (>99.999%). The liquid oxidant (LNS or  $\text{H}_2\text{O}$ ) was vaporized at room temperature, and the vaporized oxidant was introduced into the chamber without any carrier gas. A cycle of ALD consisted of the following four steps: (1) pulsing TEMAH with  $\text{N}_2$  carrier gas, (2) purging for 60 s with  $\text{N}_2$  gas (>99.999%), (3) pulsing the oxidant (LNS or  $\text{H}_2\text{O}$ ), and (4) purging for 60 s with  $\text{N}_2$  gas (>99.999%). To optimize the  $\text{HfO}_x$  ALD process involving LNS, the substrate temperature (200–400 °C), TEMAH pulse time, and LNS pulse time were varied.

### 2.2. Analyses of $\text{HfO}_x$ Thin Films Properties

The thickness of the film deposited on the Si substrate was measured using spectroscopic ellipsometry (UVISSEL, Horiba, Kyoto, Japan). XPS (Theta Probe, Thermo Fisher Scientific Co., Waltham, MA, USA) was used to analyze the chemical bonding of the  $\text{HfO}_x$

films and to ascertain the presence or absence of La in the  $\text{HfO}_x$  films. The morphological properties of the deposited films were characterized by AFM (XE-100, Park Systems, Suwon, Korea). Furthermore, the crystalline phase and crystallite size and orientation were determined by GI-XRD (SmartLab, Rigaku, Tokyo, Japan) and TEM (Tecnai F20 G<sup>2</sup>, FEI, Hillsboro, OR, USA). For the cross-sectional TEM image, a sample was prepared using the focused ion beam system, and for the plan view TEM image, samples were prepared using the ion milling system.

### 3. Results and Discussion

#### 3.1. ALD Process for $\text{HfO}_x$ Film Growth Using LNS

The characteristics of  $\text{HfO}_x$  thin films deposited using LNS as an oxidant were investigated by varying several process parameters (Figure 1a–d). Figure 1a, b show film growth saturation curves as a function of Hf-precursor (TEMAH) and LNS pulse times, respectively, with a substrate temperature of 300 °C over 50 cycles. For LNS pulse times of  $\geq 0.2$  s, the self-limiting characteristic of the reaction was apparent, as shown in Figure 1a; for these experiments, TEMAH was injected into the process chamber for more than 1 s. Figure 1b shows the film growth saturation curve as a function of LNS pulse times greater than 0.2 s. After examining Figure 1a and b, the optimized  $\text{HfO}_x$  film deposition process conditions were determined to be a substrate temperature of 300 °C, Hf-precursor pulse time of 1 s, and LNS pulse time of 0.2 s. Note that when  $\text{H}_2\text{O}$  was used as an oxidant instead of LNS, the oxidant pulse time was the same (0.2 s).

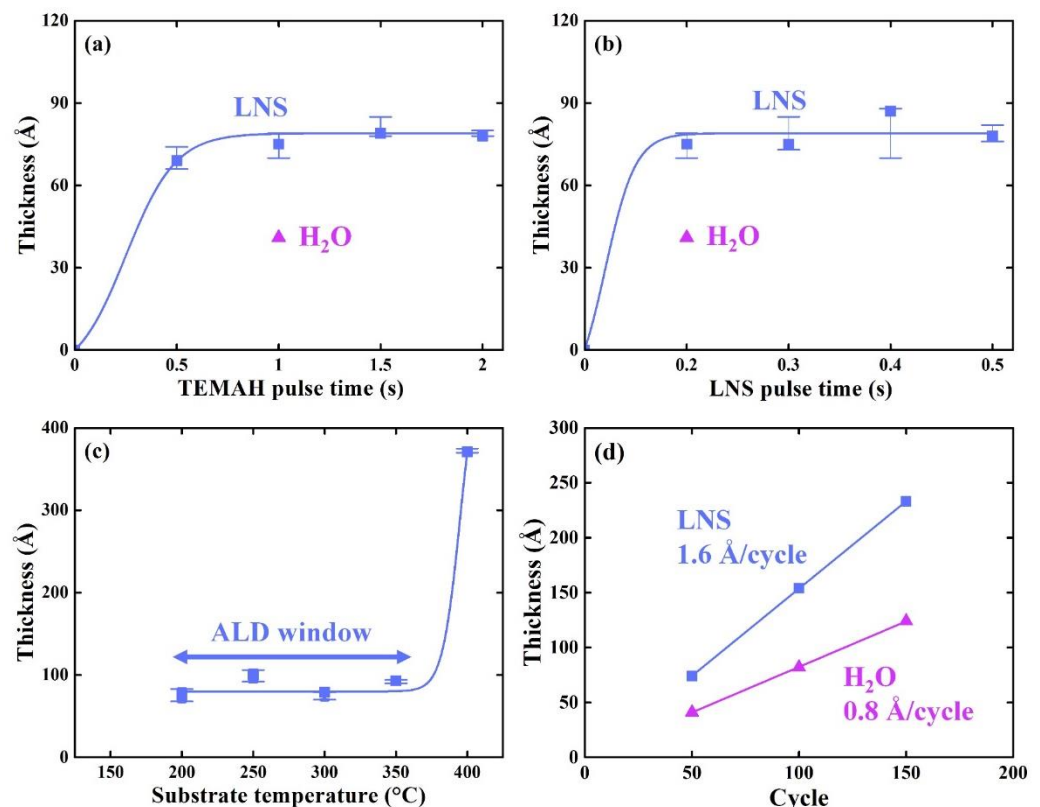


**Figure 1.** Thickness of  $\text{HfO}_x$  films grown using LNS as a function of (a) TEMAH pulse time, (b) LNS pulse time, (c) substrate temperature, and (d) ALD cycle. Data for films grown using  $\text{H}_2\text{O}$  is shown in purple for comparison in (a,b,d). The growth rates were 1.6 Å per cycle for the process involving LNS and 0.8 Å per cycle for that involving  $\text{H}_2\text{O}$ .

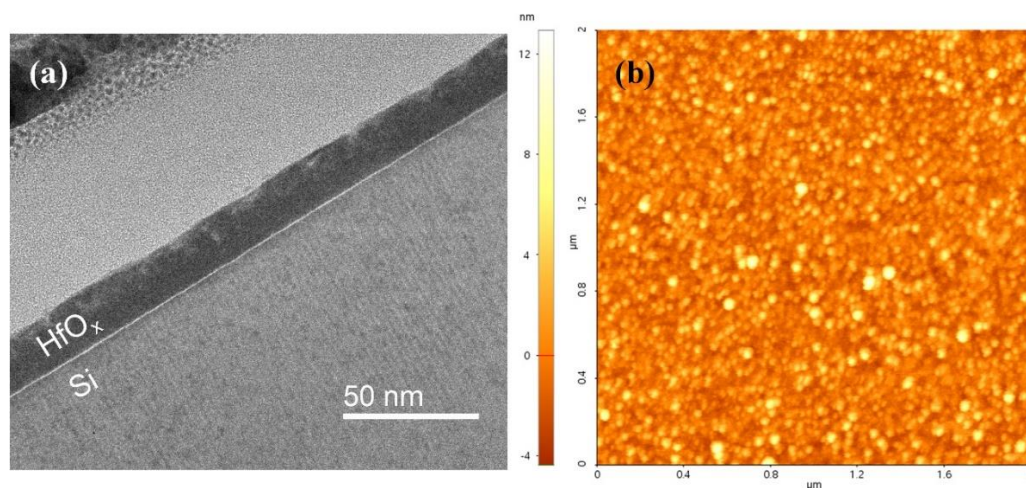
The temperature window for ALD with the TEMAH precursor and LNS oxidant was characterized by measuring the thickness of deposited  $\text{HfO}_x$  films after 50 ALD cycles as a function of the substrate temperature from 200 °C to 400 °C (Figure 1c). The ALD process

temperature window is defined as the temperature range over which a constant thickness is deposited, which was determined to be below 350 °C in this study. The temperature window for the process involving LNS was found to differ from that of the process with H<sub>2</sub>O, which was in the range of 200 °C to 400 °C [12].

HfO<sub>x</sub> films were deposited under the optimized ALD conditions—a TEMAH pulse time of 1 s, LNS pulse time of 0.2 s, and temperature of 300 °C—using various numbers of ALD cycles. As can be seen in Figure 1d, the thickness of the HfO<sub>x</sub> thin films increased linearly with the number of cycles. A HfO<sub>x</sub> growth rate of 1.6 Å per cycle was obtained with the use of the LNS oxidant. Interestingly, this rate was two times faster than that measured when H<sub>2</sub>O was used with the same pulse time (0.8 Å per cycle).

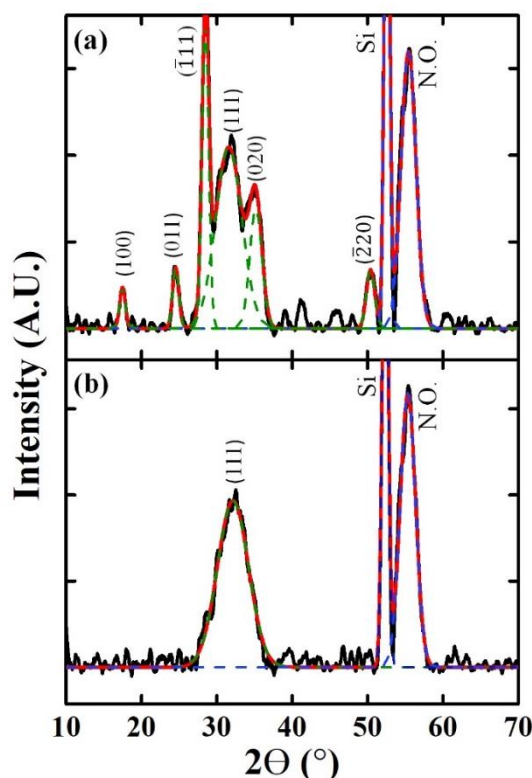
### 3.2. Microstructure of HfO<sub>x</sub> Films Prepared Using LNS

Figure 2a shows a cross-sectional TEM image of HfO<sub>x</sub> deposited on an Si substrate after 125 cycles of the optimized ALD process using LNS (TEMAH pulse time, 1 s; LNS pulse time, 0.2 s; 300 °C). The TEM image, as expected, clearly depicts an interface region consisting of native oxide (SiO<sub>x</sub>). The thickness of the HfO<sub>x</sub> film was uniform, and the average thickness was 20 nm. The surface morphology of the HfO<sub>x</sub> film is apparent in the 2 × 2 μm<sup>2</sup> AFM image in Figure 2b. The root mean square (RMS) roughness value was determined to be 1.74 nm. Finally, it should be noted that the TEM and AFM results verify that HfO<sub>x</sub> films without pinholes or cracks were successfully deposited using LNS.



**Figure 2.** (a) TEM image and (b) AFM image of 20-nm-thick HfO<sub>x</sub> film deposited on Si substrate (RMS roughness, 1.74 nm).

The crystalline phase of the deposited HfO<sub>x</sub> films on the Si substrate with optimized process parameters (TEMAH pulse time of 1 s, oxidant pulse time of 0.2 s, and temperature of 300 °C) was identified via GI-XRD. Most of the diffraction peaks of the HfO<sub>x</sub> films prepared using LNS and H<sub>2</sub>O can be assigned to the monoclinic phase (JCPDS 06-0318), in agreement with the ALD results reported in the literature (Figure 3) [13]. The result was different from that in the case of ZrO<sub>2</sub>, the phase structure of which changed from a tetragonal phase to a monoclinic phase when LNS was used [10]. For the HfO<sub>x</sub> films prepared with H<sub>2</sub>O, the normal direction of the ( $\bar{1}11$ ) plane at 28.9° was the preferred orientation, as can be clearly seen in the XRD pattern in Figure 3. In addition, the peak assigned to the (111) planes at 31.6° was broad. When LNS was used as the oxidant, a broad peak at around 32.1° appeared, which was similar to the (111) plane observed for the film prepared using H<sub>2</sub>O.



**Figure 3.** XRD patterns of  $\text{HfO}_x$  films deposited using (a)  $\text{H}_2\text{O}$  and (b) LNS. Various peak assignments are shown (N.O. indicates native oxide). The raw data and peak fitting results are shown in black and red, respectively. Green lines indicate peaks assigned to different  $\text{HfO}_x$  film orientations based on deconvolution analysis. Blue lines show Si substrates and interfacial layers. Deconvolution of the XRD patterns was performed using Gaussian functions for the shapes of the resolved peaks.

The interplanar distance and crystallite size were calculated from the angular positions of the respective preferred orientations in the XRD patterns; these values are listed in Table 1. The crystallite size of the  $\text{HfO}_x$  films was determined using the Scherrer equation,  $D = k\lambda/B\cos\theta$ , where  $\lambda$  is the XRD wavelength (1.5418 Å),  $k$  is the shape factor,  $B$  is the full width at half maximum of the measured XRD peak in radians, and  $\theta$  is the Bragg angle. A relatively small crystallite size of 1.7 nm was obtained for the  $\text{HfO}_x$  films deposited using LNS.

**Table 1.** Preferred orientations and crystallite sizes of  $\text{HfO}_x$  films deposited with  $\text{H}_2\text{O}$  and LNS.

Oxidant	Preferred Orientation	Diffraction Angle of Preferred Orientation	Crystallite Size from XRD (nm)
$\text{H}_2\text{O}$	( $\bar{1}11$ )	28.9	7.9
LNS	(111)	32.1	1.7

For more details on the difference in the crystallite size, the size of the crystallite was directly observed via dark-field TEM plan views (Figure 4). For the  $\text{HfO}_2$  films fabricated using  $\text{H}_2\text{O}$ , as shown in Figure 4a, large crystallites were observed, with diameters of more than 20 nm. In the case of the films prepared using LNS (Figure 4b), small crystallites were found with diameters of less than 10 nm. The difference between the XRD and TEM crystallite size results is likely to be related to fact that the shape factor was applied collectively. Nonetheless, the trend of smaller crystallite sizes for the films made using LNS is consistent for the results obtained via the two characterization methods.

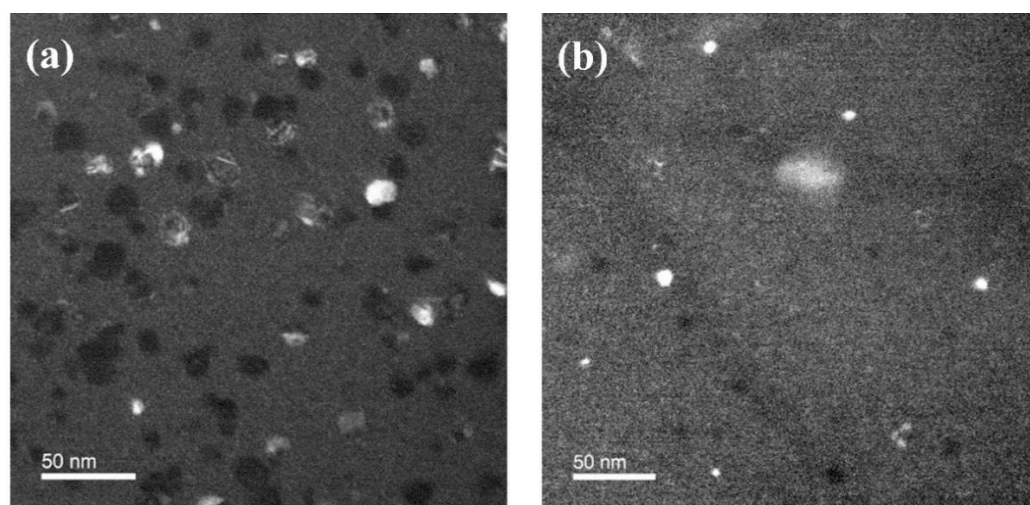


**Figure 4.** Dark-field TEM plan views of  $\text{HfO}_x$  prepared with (a)  $\text{H}_2\text{O}$  and (b) LNS films showing crystallites (black or white areas).

### 3.3. Chemical Bonding and Elemental Content of $\text{HfO}_2$ Films Deposited Using LNS

XPS analyses were carried out to determine the differences between the  $\text{HfO}_x$  films deposited using  $\text{H}_2\text{O}$  and LNS in terms of their chemical bonding characteristics and compositions. All the analyzed  $\text{HfO}_x$  films were deposited at thicknesses of up to 20 nm on Si substrates. The measured XPS results were deconvoluted using a Shirley background and Gaussian line shapes.

Figure 5a,b show Hf 4f XPS spectra of the  $\text{HfO}_x$  films deposited using  $\text{H}_2\text{O}$  and LNS, respectively. All the spectra consist of two peaks assigned to  $4f_{5/2}$  and  $4f_{7/2}$  electrons and could be fitted with two sets of the doublet peaks, for which the spin-orbit splitting was 1.68 eV. For the specimens prepared using the  $\text{H}_2\text{O}$  oxidant (Figure 5a), peaks at 16.60 eV and 18.28 eV forming one of the doublets were assigned to  $\text{Hf}^{4+} 4f_{5/2}$  and  $\text{Hf}^{4+} 4f_{7/2}$  of stoichiometric  $\text{HfO}_2$ , respectively [14,15]. The doublet at lower energy, 16.00 and 17.68 eV, was assigned to Hf suboxide ( $\text{HfO}_{2-x}$ ,  $0 < x < 2$ ), that is, the individual peaks in the doublet were assigned to  $\text{Hf}^{n+} 4f_{5/2}$  and  $\text{Hf}^{n+} 4f_{7/2}$  ( $n < 4$ ), respectively [16,17]. It is apparent from the deconvolution results that the fully oxidized  $\text{Hf}^{4+}$  doublet is much more intense than the suboxidized  $\text{Hf}^{n+}$  doublet (Figure 5a). As shown in Figure 5b, for the film prepared using LNS, the doublet assigned to stoichiometric  $\text{HfO}_2$  was located at the same binding energy as that of the film prepared using  $\text{H}_2\text{O}$  ( $\text{Hf}^{4+} 4f_{5/2}$ , 16.60 eV;  $\text{Hf}^{4+} 4f_{7/2}$ , 18.28 eV). Moreover, the positions of the peaks corresponding to  $\text{Hf}^{n+} 4f_{5/2}$  (16.15 eV) and  $\text{Hf}^{n+} 4f_{7/2}$  (17.83 eV) were similar to those for the film deposited with  $\text{H}_2\text{O}$  as the oxidant. However, the  $\text{Hf}^{4+}:\text{Hf}^{n+}$  ratio was different for the film prepared using LNS. The ratio of suboxidized  $\text{Hf}^{n+}$  was significantly increased.

Figure 5c,d show O 1s spectra of  $\text{HfO}_x$  films deposited using  $\text{H}_2\text{O}$  and LNS. These were deconvoluted into three components, respectively related to Hf–O bonding in stoichiometric  $\text{HfO}_2$ , oxygen vacancies ( $V_o$ ), and hydroxyl groups (–OH). In the spectra of both films, three peaks located at  $530.1 \pm 0.1$ ,  $531.2 \pm 0.1$ , and  $532.0 \pm 0.1$  eV, were identified by deconvolutions and assigned to H–O bonding, oxygen vacancies, and hydroxyl groups, respectively [18]. As shown in Figure 5c, for the  $\text{HfO}_x$  film deposited using  $\text{H}_2\text{O}$  as an oxidant, Hf–O bonding was found to be dominant. However, when the  $\text{HfO}_x$  film was deposited using LNS, the oxygen vacancy and hydroxyl group contents were significantly higher, as shown in Figure 5d. Non-lattice oxygen peaks, such as oxygen vacancy peaks and hydroxyl peaks, contributed to suboxide content in the oxide layer [11,19]. Thus, the O 1s XPS analysis results are in accord with the Hf 4f XPS analysis results, confirming that the  $\text{HfO}_x$  film deposited using LNS contained more suboxides.

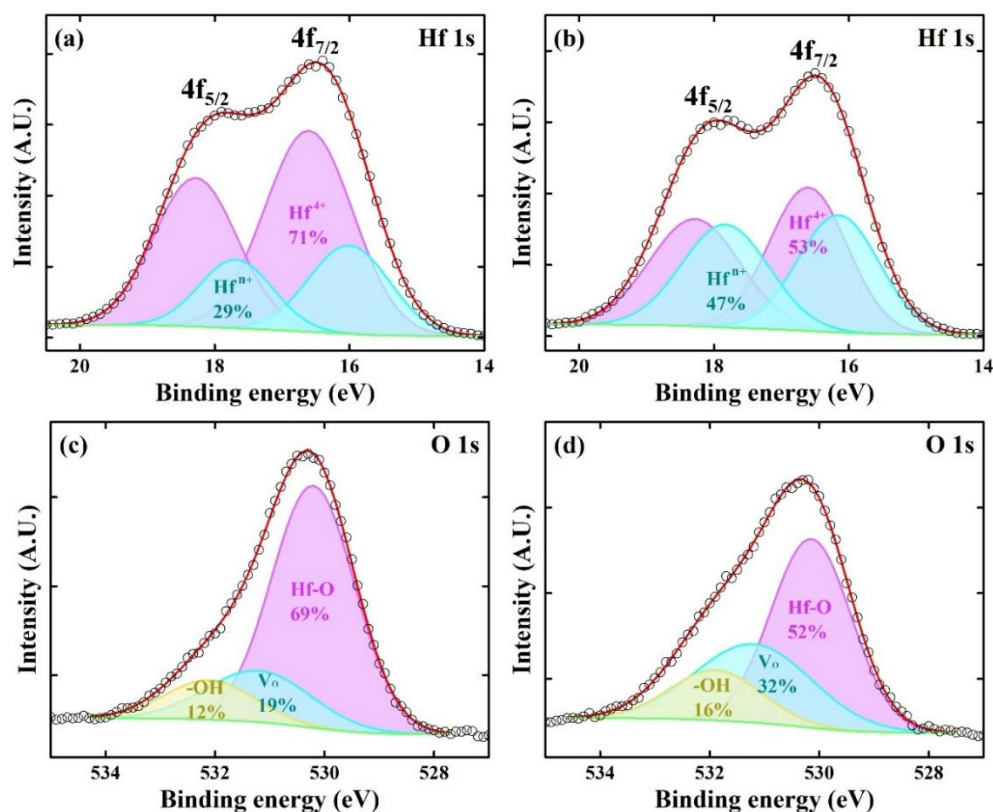


**Figure 5.** XPS results. Hf 4f spectra of HfO<sub>x</sub> films fabricated using (a) H<sub>2</sub>O and (b) LNS. O 1s spectra of HfO<sub>x</sub> films fabricated using (c) H<sub>2</sub>O and (d) LNS. The percentages are estimated values based on deconvolution analysis.

When an HfO<sub>x</sub> film prepared using LNS was utilized as a resistive switching layer, a higher current density, compared to the HfO<sub>x</sub> film prepared using H<sub>2</sub>O, was measured in the highly resistive state, indicating that these films formed more current paths [11]. The high current was caused by the increased number of grain boundaries, because of the smaller sizes of the crystallites in the films deposited with the use of LNS. The increase in the non-lattice oxygen (V<sub>o</sub>, -OH) content supplies defect states to the bandgap of oxide films. In addition, as grain boundaries are considered to be reservoirs of oxygen vacancies, the increase in the number of oxygen vacancies is expected with the increase in grain boundaries. Accordingly, the XPS results in Figure 5 are consistent with the previously reported resistive switching results [11], the XRD results as presented in Figure 3, and the TEM results presented Figure 4.

The widely reported crystalline phase of HfO<sub>x</sub> films is monoclinic. However, the doping of metal element into HfO<sub>x</sub> makes the film orthorhombic phase, showing ferroelectric characteristic. Therefore, to verify the presence or absence of La in the composition of the films, addition XPS data was analyzed. In general, in the XPS analysis for La, spin-orbit peaks of La 3d<sub>5/2</sub> and La 3d<sub>3/2</sub> appeared near 835 eV and 850 eV, respectively, and each spin-orbit component was further split via multiplet splitting [20]. However, the XPS data in Figure 6 only show background signals. It indicated that the La content was lower than the detection limit of our XPS analysis method. Thus, the results indicated that the La in the LNS oxidant hardly had very little influence on the chemical composition of the deposited HfO<sub>x</sub> films. The XRD results indicate that the HfO<sub>x</sub> existed in the monoclinic phase in the films, and the XPS results show that the La content was below the detection limit. Thus, we conclude that La in LNS is not affected by the chemical reaction with TEMAH, as observed for a ZrO<sub>2</sub> film prepared using LNS [10]. As a consequence, it can also be concluded that the HfO<sub>x</sub> deposited using LNS is probably not ferroelectric.

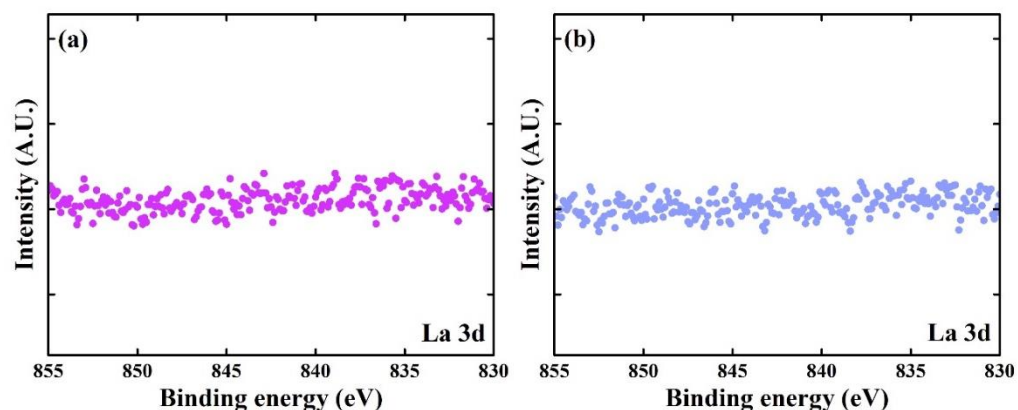


Figure 6. La 3d spectra of  $\text{HfO}_x$  films deposited using (a)  $\text{H}_2\text{O}$  and (b) LNS.

### 3.4. Relationship between Surface Energy and Crystalline Properties

It is plausible that the difference between the surface energies of the film specimens prepared using LNS and  $\text{H}_2\text{O}$  influences the differences in growth rate and crystallite size. Various research groups have investigated the relationship between surface energy and molecule adsorption. Michiardi et al. reported that when a NiTi alloy underwent oxidation, the total free energy of the alloy increased, and the increase in surface energy caused an increase in the protein adsorption [21]. Moreover, Hayami and Otani reported that in the vapor–liquid–solid process of nanowire growth, for a surface with a higher surface energy, the droplet binding energy was higher [22]. Thus, for droplet binding, the (001) plane, with the highest surface energy, is preferential. In addition, many researchers have reported the correlation of three characteristics of surface energy, orientation, and growth rate. Penn et al. reported that titanium oxide nanoparticles grow rapidly along the [001] direction, driven by the relatively high surface energy of the (001) plane [23].

Finally, we present an explanation for the correlation between the surface energy, growth rate, and crystalline characteristics of the  $\text{HfO}_x$  films. The proposed possible growth mechanisms for the  $\text{HfO}_x$  films are shown in Figure 7.

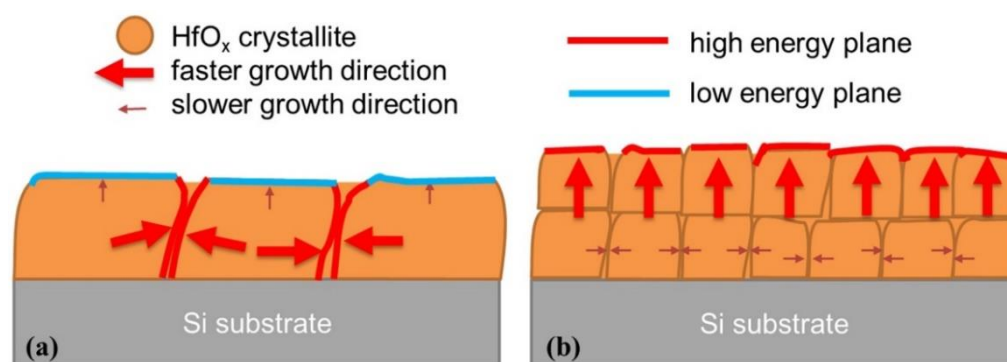


Figure 7. Schematic of  $\text{HfO}_x$  film growth using (a)  $\text{H}_2\text{O}$  and (b) LNS.

It is possible that adsorption is more favorable when the surface energy is higher. In  $\text{HfO}_x$  films, the surface energy of the (111) plane is 21% higher than that of the  $(\bar{1}\bar{1}\bar{1})$  plane [24]. When  $\text{H}_2\text{O}$  is used as an oxidant,  $\text{HfO}_x$  exists mostly as the  $(\bar{1}\bar{1}\bar{1})$  plane, which has the lowest surface energy. The low surface energy prevents the precursor from being absorbed on the surface, and hence vertical growth of the  $\text{HfO}_x$  film was slow. Meanwhile, to reduce the total free energy of the film, the size of the crystallites increases inside the film, eliminating the grain boundaries of with relatively high energies due to lattice mismatch. However, in the case of LNS, a higher surface energy favors the adsorption of the precursor to lower the total energy of the film. It can be hypothesized that differences in precursor adsorption affect the vertical growth rate of  $\text{HfO}_x$  films. In addition, high surface energies

affect the crystallization of deposited films. Owing to the high surface energy, many additional nucleation sites existed on the surface of the film. The growth of crystallites at the nucleation sites occurred via the addition of atoms from the precursor. The nuclei grow into crystallites, and the crystallites also offer a surface with high surface energy. Therefore, crystallite growth and the generation of a high-energy surface occurs cyclically. For this reason, a faster HfO<sub>x</sub> film deposition rate and smaller crystallites were observed when LNS was used in the ALD process.

#### 4. Conclusions

Nanocrystalline HfO<sub>x</sub> films were successfully synthesized by ALD using LNS. The ALD process and film characteristics were compared with those obtained when a conventional oxidant, H<sub>2</sub>O, was used. Typical ALD characteristics such as a self-limiting process, temperature window, and linear dependence of film growth on ALD cycle number were apparent. Interestingly, the growth rate when LNS was used was twice as high as that when H<sub>2</sub>O was used. The XRD results demonstrated that the HfO<sub>x</sub> films deposited with either LNS or H<sub>2</sub>O both consisted of the monoclinic phase, but there was a difference in the orientation preference. Using LNS, the preferred orientation was (111), which has a higher surface energy than the ( $\bar{1}11$ ) orientation, the preferred orientation of HfO<sub>x</sub> prepared using H<sub>2</sub>O. The TEM results revealed that the crystallite size of the HfO<sub>x</sub> film grown using LNS was smaller than that of the film grown using H<sub>2</sub>O. The XPS results showed that the HfO<sub>x</sub> films prepared using LNS had more suboxides or defects. This was consistent with the fact that the TEM results revealed a higher number of grain boundaries because of the smaller size of the crystallites. Moreover, since it was established via XPS that La dopant atoms were not present in HfO<sub>x</sub>, it is not likely that this material is ferroelectric. Finally, we suggested a growth mechanism model based on the XRD, TEM, and XPS results. It was found that the high surface energy of HfO<sub>x</sub> films grown using LNS accelerates the adsorption of the precursor and offers more nucleation sites, resulting in small crystallites and a fast growth rate.

**Author Contributions:** Conceptualization, I.-S.P.; methodology, S.Y.K. and Y.C.J.; formal analysis, S.Y.K., Y.C.J., S.S., I.-S.P., T.L. and J.A.; investigation, S.Y.K. and Y.C.J.; writing—original draft preparation, S.Y.K.; writing—review and editing, I.-S.P. and J.A.; funding acquisition, I.-S.P. and J.A. All authors have read and agreed to the published version of the manuscript.

**Funding:** This research was supported by the Creative Materials Discovery Program on Creative Multilevel Research Center (No. 2015M3D1A1068061) and National R&D Program (NRF-2020M3H4A3081881) through the National Research Foundation of Korea (NRF) funded by Ministry of Science and ICT.

**Conflicts of Interest:** The authors declare no conflict of interest.

#### References

1. Tsai, Y.-H.; Chou, C.-H.; Chung, Y.-Y.; Yeh, W.-K.; Lin, Y.-H.; Ko, F.-H.; Chien, C.-H. Demonstration of HfO<sub>2</sub>-based gate dielectric with low interface state density and sub-nm EOT on Ge by incorporating Ti into interfacial layer. *IEEE Electron Device Lett.* **2019**, *40*, 174–176. [[CrossRef](#)]
2. Jung, Y.C.; Seong, S.; Lee, T.; Kim, S.Y.; Park, I.-S.; Ahn, J. Improved resistive switching characteristics of a Pt/HfO<sub>2</sub>/Pt resistor by controlling anode interface with forming and switching polarity. *Appl. Surf. Sci.* **2018**, *435*, 117–121. [[CrossRef](#)]
3. Schroeder, U.; Richter, C.; Park, M.H.; Schenk, T.; Pesic, M.; Hoffmann, M.; Fengler, F.P.G.; Pohl, D.; Rellinghaus, B.; Zhou, C.; et al. Lanthanum-doped hafnium oxide: A robust ferroelectric material. *Inorg. Chem.* **2018**, *57*, 2752–2765. [[CrossRef](#)] [[PubMed](#)]
4. Fan, Z.; Chen, J.; Wang, J. Ferroelectric HfO<sub>2</sub>-based materials for next-generation ferroelectric memories. *J. Adv. Dielectr.* **2016**, *6*, 1630003. [[CrossRef](#)]
5. Johnson, R.W.; Hultqvist, A.; Bent, S.F. A brief review of atomic layer deposition: From fundamentals to applications. *Mater. Today* **2014**, *17*, 236–246. [[CrossRef](#)]
6. Park, I.-S.; Jung, Y.C.; Seong, S.; Ahn, J.; Kang, J.; Noh, W.; Lansalot-Matras, C. Atomic layer deposition of Y<sub>2</sub>O<sub>3</sub> films using heteroleptic liquid (iPrCp)<sub>2</sub>Y(iPr-amd) precursor. *J. Mater. Chem. C* **2014**, *2*, 9240–9247. [[CrossRef](#)]
7. Granneman, E.; Fischer, P.; Pierreux, D.; Terhorst, H.; Zagwijn, P. Batch ALD: Characteristics, comparison with single wafer ALD, and examples. *Surf. Coat. Tech.* **2007**, *201*, 8899–8907. [[CrossRef](#)]

8. Muñoz-Rojas, D.; Huong Nguyen, V.; Masse de la Huerta, C.; Jiménez, C.; Bellet, D. Spatial Atomic Layer Deposition. In *Chemical Vapor Deposition for Nanotechnology*; Mandracci, P., Ed.; IntechOpen: London, UK, 2019; pp. 1–25.
9. Januar, M.; Prakoso, S.P.; Lan, S.-Y.; Mahanty, R.K.; Kuo, S.-Y.; Liu, K.-C. The role of oxygen plasma in the formation of oxygen defects in HfO<sub>x</sub> films deposited at room temperature. *J. Mater. Chem. C* **2015**, *3*, 4104–4114. [[CrossRef](#)]
10. Oh, N.K.; Kim, J.-T.; Kang, G.; An, J.-K.; Nam, M.; Kim, S.Y.; Park, I.-S.; Yun, J.-Y. Oxidant effect of La(NO<sub>3</sub>)<sub>3</sub>·6H<sub>2</sub>O solution on the crystalline characteristics of nanocrystalline ZrO<sub>2</sub> films grown by atomic layer deposition. *Appl. Surf. Sci.* **2017**, *394*, 231–239. [[CrossRef](#)]
11. Jung, Y.C.; Park, I.-S.; Seong, S.; Lee, T.; Kim, S.Y.; Ahn, J. Enhanced resistive switching characteristics of HfO<sub>x</sub> insulator fabricated by atomic layer deposition and La(NO<sub>3</sub>)<sub>3</sub>·6H<sub>2</sub>O solution as catalytic oxidant. *J. Vac. Sci. Technol. A* **2020**, *38*, 032405. [[CrossRef](#)]
12. Park, I.-S.; Lee, T.; Choi, D.-K.; Ahn, J. Metal precursor effects on deposition and interfacial characteristics of HfO<sub>2</sub> dielectrics grown by atomic layer deposition. *J. Korean Phys. Soc.* **2006**, *49*, S544–S547.
13. Chiou, Y.-K.; Chang, C.-H.; Wu, T.-B. Characteristics of hafnium oxide grown on silicon by atomic-layer deposition using tetrakis(ethylmethylamino)hafnium and water vapor as precursors. *J. Mater. Res.* **2007**, *22*, 1899–1906. [[CrossRef](#)]
14. Jung, Y.C.; Seong, S.; Lee, T.; Kim, S.Y.; Park, I.-S.; Ahn, J. Effects of hydrogen annealing temperature on the resistive switching characteristics of HfO<sub>x</sub> thin films. *Mater. Sci. Semicond. Process.* **2018**, *88*, 207–213. [[CrossRef](#)]
15. Barreca, D.; Milanov, A.; Fischer, R.A.; Devi, A.; Tondello, E. Hafnium oxide thin film grown by ALD: An XPS study. *Surf. Sci. Spectra* **2007**, *14*, 34–40. [[CrossRef](#)]
16. Tan, T.; Guo, T.; Wu, Z.; Liu, Z. Charge transport and bipolar switching mechanism in a Cu/HfO<sub>2</sub>/Pt resistive switching cell. *Chin. Phys. B* **2016**, *25*, 117306. [[CrossRef](#)]
17. Zhang, W.; Kong, J.-Z.; Cao, Z.-Y.; Li, A.-D.; Wang, L.-G.; Zhu, L.; Li, X.; Cao, Y.-Q.; Wu, D. Bipolar resistive switching characteristics of HfO<sub>2</sub>/TiO<sub>2</sub>/HfO<sub>2</sub> trilayer-structure RRAM devices on Pt and TiN-coated substrates fabricated by atomic layer deposition. *Nanoscale Res. Lett.* **2017**, *12*, 393. [[CrossRef](#)] [[PubMed](#)]
18. Chung, J.; Tak, Y.J.; Kim, W.-G.; Park, J.W.; Kim, T.S.; Lim, J.H.; Kim, H.J. Low-temperature fabrication of solution-processed hafnium oxide gate insulator films using a thermally purified solution process. *J. Mater. Chem. C* **2018**, *6*, 4928–4935. [[CrossRef](#)]
19. Luo, X.; Li, Y.; Yang, H.; Liang, Y.; He, K.; Sun, W.; Lin, H.-H.; Yao, S.; Lu, X.; Wan, L.; et al. Investigation of HfO<sub>2</sub> thin films on Si by X-ray photoelectron spectroscopy, Rutherford backscattering, grazing incidence X-ray diffraction and variable angle spectroscopic ellipsometry. *Crystals* **2018**, *8*, 248. [[CrossRef](#)]
20. Atuchin, V.V.; Kalinkin, A.V.; Kochubey, V.A.; Kruchinin, V.N.; Vemuri, R.S.; Ramana, C.V. Spectroscopic ellipsometry and x-ray photoelectron spectroscopy of La<sub>2</sub>O<sub>3</sub> thin films deposited by reactive magnetron sputtering. *J. Vac. Sci. Technol. A* **2011**, *29*, 021004. [[CrossRef](#)]
21. Michiardi, A.; Aparicio, C.; Ratner, B.D.; Planell, J.A.; Gil, J. The influence of surface energy on competitive protein adsorption on oxidized NiTi surfaces. *Biomaterials* **2007**, *28*, 586–594. [[CrossRef](#)] [[PubMed](#)]
22. Hayami, W.; Otani, S. The role of surface energy in the growth of boron crystals. *J. Phys. Chem. C* **2007**, *111*, 688–692. [[CrossRef](#)]
23. Penn, R.L.; Banfield, J.F. Morphology development and crystal growth in nanocrystalline aggregates under hydrothermal conditions: Insight from titania. *Geochim. Cosmochim. Acta* **1999**, *63*, 1549–1557. [[CrossRef](#)]
24. Mukhopadhyay, A.B.; Sanz, J.F.; Musgrave, C.B. First-principles calculations of structural and electronic properties of monoclinic hafnia surfaces. *Phys. Rev. B* **2006**, *73*, 115330. [[CrossRef](#)]